Journal of
Applied Crystallography

ISSN 0021-8898

Received 15 August 2006
Accepted 11 January 2007

Self-assembled films of hydrophobin protein HFBIII from *Trichoderma reesei*

Kaisa Kisko,[a]* Géza R. Szilvay,[b,c] Elina Vuorimaa,[d] Helge Lemmetyinen,[d] Markus B. Linder,[b] Mika Torkkeli[a] and Ritva Serimaa[a]

[a]Department of Physical Sciences, POB 64, 00014 University of Helsinki, Finland, [b]VTT Biotechnology, POB 1400, 02044 VTT, Finland, [c]Programme for Structural Biology and Biophysics, Institute of Biotechnology, 00014 University of Helsinki, Finland, and [d]Department of Materials Chemistry, POB 541, 33101 Tampere University of Technology, Finland. Correspondence e-mail: kaisa.kisko@helsinki.fi

Hydrophobins are a group of small amphiphilic proteins which are known to self-assemble on interfaces. They contain eight conserved cysteine residues, which make four disulfide bridges. A new hydrophobin protein, HFBIII, from the fungus *Trichoderma reesei* contains one extra cysteine residue, giving the protein a naturally reactive site. The self-assembly of hydrophobin protein HFBIII was studied using grazing-incidence X-ray diffraction and reflectivity. HFBIII self-assembles into a hexagonally ordered monolayer at an air/water interface and also forms crystalline coatings on a silicon substrate. The lattice constants for the hexagonal coatings are $a = b = 56.5$ Å, $\gamma = 120^\circ$. The self-assembled structure in the HFBIII film is very similar to those formed by two other *T. reesei* hydrophobins, HFBI and HFBII.

1. Introduction

Self-assembly of proteins is ubiquitous in nature. Proteins interact with each other and their environment to organize into functional units. Self-assembly is a complex process involving hydrogen bonds, electrostatic interactions, van der Waals forces and hydrophobic interactions. In the laboratory, self-assembly can be used in the synthesis of functional nanomaterials and devices (Zhang, 2003).

Hydrophobins are a group of small fungal proteins with remarkable surface-chemical properties (Linder *et al.*, 2005). These arise from the amphiphilic structure of the proteins, where the hydrophobic and hydrophilic parts are separated (Hakanpää, Paananen, Askolin *et al.*, 2004; Kwan *et al.*, 2006). Hydrophobins lower the surface tension of water even down to one third (Wösten *et al.*, 1999; Askolin *et al.*, 2006), adhere to various surfaces and self-assemble on hydrophobic/hydrophilic interfaces. This self-assembly has been demonstrated, for example, on interfaces between air and water, oil and water, and hydrophobic solid and water (Wösten *et al.*, 1994; Askolin *et al.*, 2006).

Hydrophobins have various roles in fungal life and development. Hydrophobins enable the growth of aerial stuctures by lowering the surface tension of water (Wösten *et al.*, 1999). They coat the aerial structures and spores (Wösten *et al.*, 1993), and are also present in the cell walls (van Wetter *et al.*, 2000). Hydrophobins are divided into two classes based on their hydropathy patterns and solubility of aggregates (Wessels, 1994). The above mentioned properties are common to both class I and class II hydrophobins. The work here concerns hydrophobins of class II.

Class II hydrophobins from the fungus *Trichoderma reesei* have been extensively studied during the past ten years. The genome of *T. reesei* contains several hydrophobin genes. From these, two proteins, HFBI and HFBII, have been previously isolated, purified and characterized (Nakari-Setälä *et al.*, 1996, 1997). HFBI is involved in hyphal development and HFBII in sporulation (Askolin *et al.*, 2005). The aggregation of HFBI and HFBII has been studied using X-rays and atomic force microscopy. According to X-ray crystallography the HFBII monomer is spherical (Hakanpää, Paananen, Askolin *et al.*, 2004). Based on small-angle X-ray scattering results both HFBI and HFBII exist as tetramers in solution (Torkkeli *et al.*, 2002) in concentrations of 10–100 mg ml^{-1}. In lower concentrations the tetramers dissociate into dimers and monomers (Szilvay *et al.*, 2006). HFBI and HFBII self-assemble on an air/water interface into a hexagonally ordered coating (Kisko *et al.*, 2007). They also form ordered monolayer and multilayer Langmuir–Blodgett films (Paananen *et al.*, 2003; Kisko *et al.*, 2005).

Here we present the first structural studies of hydrophobin HFBIII from *T. reesei*. A typical feature of all hydrophobins is that they contain a conserved pattern of eight cysteine residues, which create four disulfide bridges. HFBIII, however, contains one extra cysteine residue, creating a naturally active site in the protein. Despite this difference HFBIII can be classified as a hydrophobin, because the positions of all the other cysteine residues are conserved (the same as in HFBI and HFBII) (Linder *et al.*, 2005).

We studied self-assembled films of HFBIII on an air/water interface and on a silicon substrate. These self-assembled films were characterized using grazing-incidence X-ray diffraction (GID) and reflectivity. Grazing-incidence X-ray diffraction has been used for *in situ* structural studies of Langmuir films (Als-Nielsen *et al.*, 1994) and two-dimensional protein crystals on air/water interfaces (Haas *et al.*, 1995; Verclas *et al.*, 1999). The best resolution achieved with two-dimensional protein crystals is about 10 Å (Lenne *et al.*, 2000).

2. Experimental

2.1. Sample preparation

The protein HFBIII (Linder *et al.*, 2005) was purified from the mycelium of an *hfb3* overexpressing *T. reesei* strain (E. Rintala & T.

Nakari-Setälä, unpublished results), essentially as described for HFBI (Linder *et al.*, 2001). The identity of the protein was determined with matrix-assisted laser desorption ionization/time-of-flight mass analysis (Institute of Biotechnology, University of Helsinki, Finland) and quantitative amino-acid analysis (Amino Acid Analysis Laboratory, Uppsala University, Sweden) (M. Linder, unpublished results).

2.2. Measurements on the air/water interface

The measurements on the air/water interface were conducted at the European Synchrotron Radiation Facility (ESRF) at beamline ID10B. The beam was monochromated to an energy of 7.993 keV with a diamond(111) double-crystal monochromator and deflected to the air/water interface using a Ge(111) crystal. The beam size was reduced with slits to be 0.5 × 0.1 mm (horizontal × vertical) on the sample position. The angle of incidence was 0.12°, which is 80% of the critical angle of total internal reflection of water. The diffraction pattern was collected by scanning a vertically aligned Soller-collimated 50 mm Braun linear position-sensitive detector over a 2θ range of 1.5–10° with a step of 0.025°. The angular range in the vertical direction was α_f = 0–12°. The measurement time for one image was approximately 1 h. The measurements were conducted as a function of pressure in a Langmuir trough (170 × 438 mm, 3 mm deep). Aqueous 1 m*M* acetate buffer (pH 5.0) was used as a subphase. The temperature of the subphase was 293.2 ± 0.3 K. The 30 µ*M* hydrophobin solution was allowed to incubate for 24 h before spreading on the subphase. The trough was covered and thereafter constantly flushed with humidified helium. The measurements were started when the oxygen level had decreased to 10% of the original value, which helped to minimize the background and reduce possible radiation damage. Furthermore, after each 1 h measurement the irradiated area was changed. No effects of radiation damage on the sample or on its diffraction pattern were seen.

The surface pressure was controlled using a barrier on one side of the trough and recorded using a Wilhelmy balance. The compression speed was 17 cm^2 min^{-1}. For the measurement at 0 mN m^{-1}, 67 µl of the hydrophobin solution was spread to yield a very high mean molecular area. For the rest of the measurements the volume was 580 µl and the pressure was increased in steps of 5–10 mN m^{-1} and kept constant during the measurements. The mean molecular areas at each pressure are shown in Fig. 1 with the full isotherm of HFBIII (see below). The changes in the mean molecular areas during the 1 h of the measurements were about 10 Å^2.

The full isotherm of HFBIII was measured with a KSV minitrough (KSV Instruments Ltd). Aqueous 1 m*M* acetate buffer (pH 5.0) was used as a subphase. The temperature of the subphase was 291.0 ± 0.5 K. The surface pressure was recorded using a Wilhelmy balance. The compression speed was 4.5 cm^2 min^{-1}. 200 µl of the 30 m*M* hydrophobin solution was spread on the air–water interface and allowed to stabilize for 20 min before compression. The initial pressure was 0.62 mN m^{-1}.

2.3. Measurements on the silicon substrate

The self-assembled films on the silicon substrate were measured at the wiggler beamline W1.1 at the synchrotron radiation facility HASYLAB/DESY. The incoming beam was monochromated using an Si(111) double-crystal monochromator to an energy of 8.048 keV. The beam was reduced with slits to be 0.5 × 0.1 mm (horizontal × vertical) for the GID measurements and 1 × 0.1 mm for the reflectivity scans. In the GID measurements the angle of incidence was 0.155°. The GID patterns were recorded using a Molecular Dynamics image-plate detector mounted on the diffractometer arm 31 cm from the sample. The angular range was calibrated using a silver behenate standard sample. The reflectivity patterns were collected using a scintillation counter. The measurement times were 30 min for GID and 10 min for the reflectivity. During the measurements the sample was kept under a constant helium flow in order to reduce the background and radiation damage.

For measurements of HFBIII assemblies in the dry state, a silicon substrate was used. The native oxide layer of an Si(110) substrate was removed with hydrofluoric acid to obtain a hydrophobic surface. Immediately after the treatment, 0.5 ml of a 50 µg ml^{-1} HFBIII solution in water was pipetted on the surface and allowed to dry completely. The measurements were performed at 298 K.

3. Results

3.1. On the air/water interface

According to GID results HFBIII self-assembles into a hexagonally ordered coating on the air/water interface. Crystalline rafts are

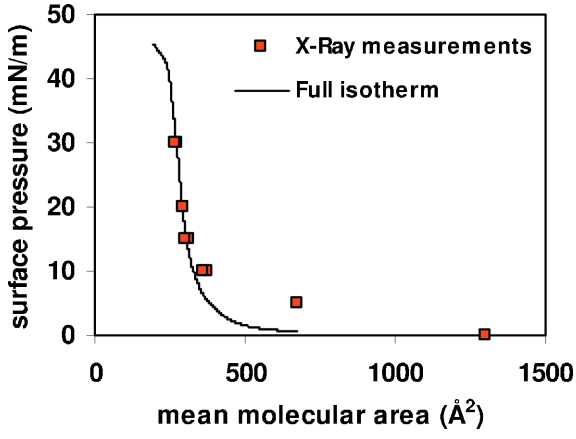

Figure 1
The full isotherm of HFBIII and the mean molecular areas corresponding to the surface pressure at each GID measurement. The differences in the small surface pressures are due to the different surface areas of the troughs used.

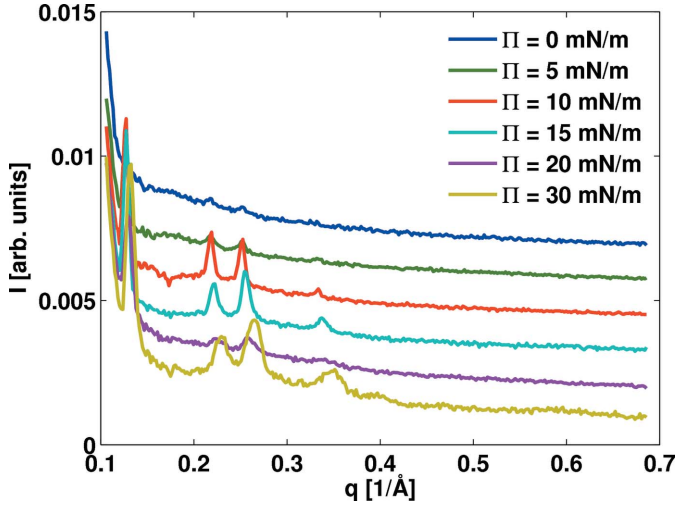

Figure 2
Diffraction pattern of HFBIII at the air/water interface as a function of surface pressure Π. The lowest pressure is at the top. The intensities have been integrated over the angular range $0 < \alpha_f < 1°$.

spontaneously formed at zero surface pressure. In Fig. 2 the diffraction patterns integrated over the range of $0 < \alpha_f < 1^\circ$ (where α_f is the vertical exit angle) are shown as a function of the pressure. For comparison, the top part of Fig. 5 shows the complete two-dimensional diffraction pattern measured at a surface pressure of Π = 15 mN m^{-1}. In both diffraction patterns the length of the scattering vector was defined as $q = (4\pi/\lambda)\sin\theta$, where θ is half of the scattering angle and λ is the wavelength.

At zero surface pressure the peaks, or Bragg rods, are faint. Their positions correspond to a hexagonal structure with $a = b = 57.5$ Å, $\gamma = 120^\circ$. As the surface pressure is increased, the intensities of the peaks increase. Their positions shift to slightly larger angles, corresponding a decrease of a from 57.5 to 55.0 Å. These changes in the intensity and the size of the unit cell as a function of pressure are not very systematic. Repeated measurements from a different position in the Langmuir trough gave the same peaks but different intensities. It is well known that compression of a monolayer at the air/water interface gives rise to domains (Leporatti *et al.*, 2000; Chen *et al.*, 2005). These domains tend to fuse during compression and give rise to a more compact monolayer. At zero pressure the HFBIII protein molecules are on average far away from each other. However, it seems that the tendency to form an organized layer at the air–water interface is so strong for these proteins that they form crystalline domains already at zero surface pressure. This nucleation of the domains takes place in a number of positions leading to small crystallites rather far away from each other. There can be amorphous material between the crystalline domains, as was seen in Langmuir–Blodgett films of the hydrophobin protein HFBII on a solid substrate (Paananen *et al.*, 2003). Thus the measured intensity can vary from one position to another.

As the pressure is increased and the crystallites are forced closer to each other they can start to fuse, giving rise to larger crystallites. However, the number of peaks in the diffraction pattern remains constant, so the ordering does not seem to be improving. Furthermore, the intensity variations along the peaks remain unchanged, which implies that the arrangment of the protein molecules within the unit cell does not change as a function of pressure.

3.2. On the silicon substrate

The diffraction pattern of a dried film of HFBIII on a silicon substrate is shown in Fig. 3. The film is again hexagonally ordered with $a = b = 56.5$ Å, $\gamma = 120^\circ$. The size of the unit cell is almost equal on the air/water interface and on the solid substrate. The Bragg rods in the dried film are very elongated, but unfortunately too faint to allow more detailed modelling.

X-ray reflectivity was used to study the thickness of the dried film, its (electron) density and the roughnesses of the air/film and film/substrate interfaces. The reflectivity curve (Fig. 4) shows oscillations arising from the hydrophobin film. The reflectivity was modelled using a box-model (insert in Fig. 4) and fitted with a program (Seeck *et al.*, 2000) that uses the Parrat formalism (Parrat, 1954). The thickness of the hydrophobin film, its electron density and the interfacial roughnesess were fitting parameters. The experimental conditions, such as the footprint of the beam on the sample, were also taken into account. According to the fit the thickness of the film is 91 Å. The inhomogeneities in the film structure and in the electron-density profile cause the slight deviations of the fit from the experimental data.

4. Modelling

For further analysis of the arrangement of the HFBIII proteins inside the unit cell, the grazing-incidence diffraction patterns were modelled using the program *IsGISAXS* (Lazzari, 2002). The program is intended for the simulation and analysis of islands supported on or buried inside a substrate. The island shape, the interference function between islands and the experimental parameters are given as input. The program uses the distorted-wave Born approximation (DWBA) for computation of the intensity.

In the calculation of the model intensity, the islands were thought to represent HFBIII monomers or aggregates. These islands formed the hexagonal lattice. Various different island shapes, such as cylinders, boxes, spheres, hemispheres and ellipsoids with different aspect ratios, were tested. The best agreement with the experimental pattern was obtained using an ellipsoid, with one island per unit cell. Fig. 5 shows the comparison between an ellipsoidal *IsGISAXS* model (middle part) and the experimental diffraction pattern of HFBIII on the air/water interface at a surface pressure of 15 mN m^{-1} (top part). In the model, the width of the island is 50 Å, the diameter is 65 Å and the height is 30.5 Å (Fig. 5). The electron density of the particle was approximated by the electron density of HFBII. The two-dimensional pattern was calculated for a hexagonal lattice with a lattice constant a = 56 Å using the local monodisperse approximation.

The positions of the Bragg rods are well reproduced by the model, but the variation of the intensity along them does not quite follow the data. The differences can arise from some simplifications used in the model. The shapes of the islands are restricted to simple geometrical objects and the electron density within the islands is assumed to be constant. More importantly, in the program all the islands are lying on the same level. Lifting some of the protein molecules in the unit cell relative to the others affects the intensity variation along the Bragg rods (Kmetko *et al.*, 2001) and could thus produce a better match with the experiment. To test this possibility we generated model systems and calculated the intensity profiles of the Bragg rods *hk* using the structure factor

$$F_{hk}(q_z) = \sum_j f_j \exp\left[2\pi i(hx_j + ky_j) + iq_z z_j\right], \quad (1)$$

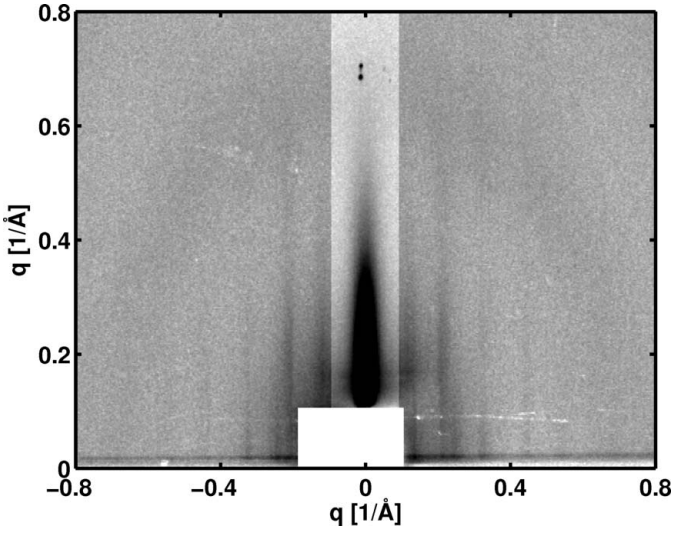

Figure 3
Dried film of HFBIII on a silicon surface. The intensity in the middle part has been divided by 2 for clarity.

where f_j is the form factor of the atom j, whose fractional coordinates in the two-dimensional unit cell are (x_j, y_j). z_j is the height (not in the coordinates of the unit cell). The folded structure of HFBIII, and thus the positions of the individual atoms, is not known, but because monomers of both HFBI (Hakanpää *et al.*, 2006) and HFBII (Hakanpää, Paananen, Askolin *et al.*, 2004) are rather spherical, HFBIII was approximated by a sphere. The HFBIII spheres were generated in various hexagonal space groups and the number, position and radius of the spheres were varied. Fig. 5 (bottom part) shows a good fit obtained using six monomers of radius $R = 9$ Å per unit cell in space group $P6_5$. The space group has a sixfold screw axis and each protein molecule is lifted by (1/6)c relative to the previous one. The length of the c axis is 22 Å. The first sphere is positioned at (0.2, 0.3). The second sphere is obtained by lifting the first one by 3.6 Å and rotating it by 60° around the c axis. There are six monomers altogether in each ring, so the film is one unit cell thick. The total height of the film is then $2R + [(5/6) \times 22] = 36$ Å. Addition of further layers or unit cells gives sharper maxima in the Bragg rods.

5. Discussion

Self-assembled films of HFBIII on the air/water interface and on the silicon substrate were prepared using different methods. On one hand, the film on the air/water interface was prepared by spreading hydrophobin solution onto the Langmuir trough. At zero surface pressure the mean molecular area was as large as 1300 Å^2, but the molecules still self-assembled into crystalline domains. On the other hand, the film on the solid substrate was obtained by evaporating a droplet of hydrophobin solution on to the silicon substrate. During the slow evaporation, the molecules were forced close to each other and formed an ordered coating. Interestingly, in both cases HFBIII formed hexagonally ordered films. The thickness of the film on the air/water interface, as estimated from the *IsGISAXS* model, is about 31 Å. The structure-factor computation gives a value of 36 Å for the total thickness of the film. This film can be seen as a monolayer, because the protein molecules are not on top of each other.

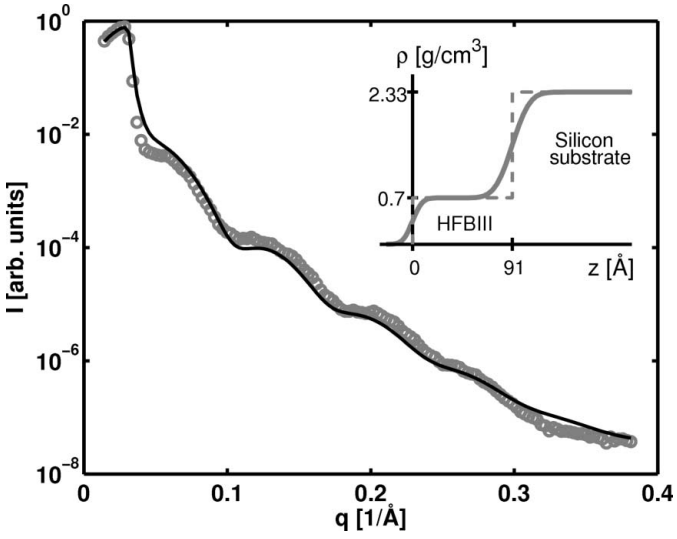

Figure 4
Reflectivity curve of a dried film of HFBIII and a fit using a box model for the electron density (insert) (Seeck *et al.*, 2000). In the fit the thickness of the hydrophobin film is 91 Å. The roughnesses of the interfaces are described by a Gaussian function with $\sigma_{air/film} = 6.9$ Å and $\sigma_{film/Si} = 12.5$ Å. The (electron) density of the hydrophobin film was also treated as a fitting parameter.

According to the reflectivity data, the thickness of the dried HFBIII film is about 90 Å, so this film is clearly a multilayer of protein molecules. The thickness is determined by the concentration and size of the original droplet.

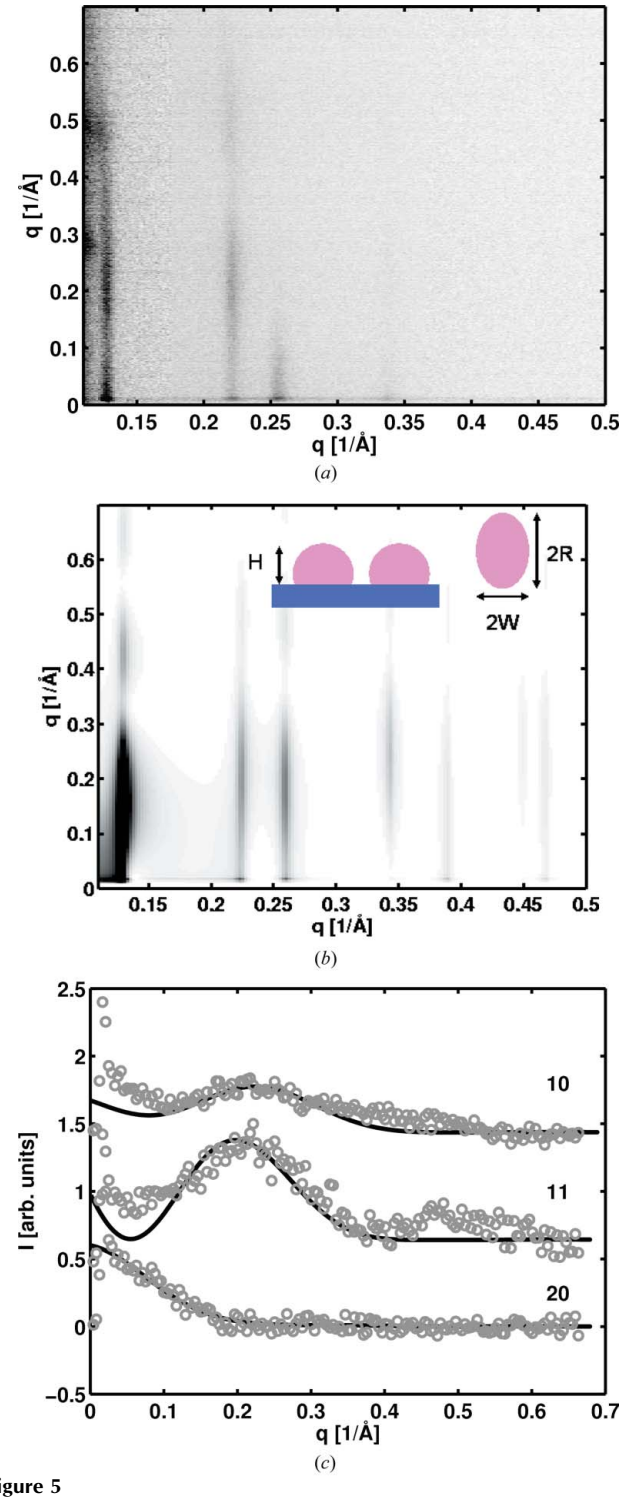

Figure 5
Top part: the two-dimensional diffraction pattern of HFBIII at a surface pressure of 15 mN m^{-1}. Middle part: the *IsGISAXS* model. The insert shows the notation of the ellipsoidal islands on the air/water interface used for the calculation. Here W = 25, R = 32.5 and H = 30.5 Å. Bottom part: the intensity profiles of the first three Bragg rods and the model computed in space group $P6_5$. The background has been subtracted from the profiles.

The hydrophobin films on the air/water interface and on the solid substrate resemble each other. Both have the same crystal structure with similar unit-cell dimensions. Furthermore, the intensity variations along the Bragg rods have certain similarities, such as a fast decaying third peak at $q = 0.26$ Å^{-1} (see Fig. 5). The similarities imply that the organization of the protein molecules in both films is similar. The faint Bragg rods in the dried film are very elongated. This suggests that the thickness of the crystalline layer is small. Below it there can be amorphous materials adsorbed to the substrate. During the slow evaporation, part of the hydrophobins self-assemble on the air/water interface. Apparently the protein molecules remaining in the solution attach to this layer, which determines the overall crystalline structure of the film.

We used both the program *IsGISAXS* and a direct computation of the structure factor for model systems to simulate the data. The *IsGISAXS* program provided useful information on the aggregation of the protein molecules. According to the *IsGISAXS* model, the height of the protein island was 30.5 Å, which is slightly larger than the diameter of an HFBI or HFBII monomer. The other dimensions of the island are larger, and so one island does not represent a monomer but a larger aggregate. The surface area of the island facing the water is 2553 Å^2, so up to six spheres of radius $R = 11$ Å would fit inside it, as would the hexagonal ring calculated using equation (1). In this way, the *IsGISAXS* result can be seen as a low-resolution model. The fit of the *IsGISAXS* model to the data is rather poor. This shows that the data cannot be described by a flat model, in which all the molecules are on the same level. The data analysis was continued by calculating for some model systems the intensity profiles along the three first peaks. The result presented in Fig. 5 provided a good fit to the experimental data, but almost as good fits could also be obtained using different arrangements of the monomers. As long as there is no information on the structure of the HFBIII monomer, the model remains tentative.

Previously the program *IsGISAXS* has been used for simulations of inorganic systems, such as nanoparticles on a substrate (Renaud *et al.*, 2003), or for thin polymer films (Müller-Buschbaum *et al.*, 2004). However, as demonstrated here, it also provides a useful tool for analysis of two-dimensional protein structures.

The water subphase for the measurements on the air/water interface contained sodium acetate buffer, whereas the film on the silicon substrate was evaporated from pure water solution without a buffer. Under both conditions the proteins self-assembled into an ordered film, which means that the crystallization occurs irrespective of the ionic interactions with the buffer. In previously studied multilayer Langmuir–Blodgett films, HFBI and HFBII proteins also formed hexagonal crystallites with lattice constants $a = 54$ Å for HFBI and $a = 55$ Å for HFBII (Kisko *et al.*, 2005). However, the addition of salt can change the behaviour: when HFBI and HFBII were dehydrated from a solution containing salt onto native silicon (Ritva *et al.*, 2003), the HFBI film was weakly ordered whereas HFBII formed a highly crystalline film, whose structure changed from monoclinic to hexagonal upon drying. The hexagonal unit cell was smaller than in other cases, with $a = 38.7$ Å. A similar phenomenom is also observed with three-dimensional single crystals. According to protein-crystallography studies, HFBI (Askolin *et al.*, 2004; Hakanpää *et al.*, 2006) and HFBII (Hakanpää, Paananen, Askolin *et al.*, 2004; Hakanpää, Parkkinen, Hakulinen *et al.*, 2004) can crystallize into different crystal structures depending on the conditions, *i.e.* with salts or detergents. This highlights the complexity of interactions and their delicate balance in the formation of protein films and crystals.

The amino-acid sequence of HFBIII (Linder *et al.*, 2005) is 45% identical to both HFBI and HFBII. The positions of the eight cysteine residues in HFBI and HFBII are the same in HFBIII (Linder *et al.*, 2005). According to protein crystallography of HFBII crystallized in the presence of manganese (Hakanpää, Paananen, Askolin *et al.*, 2004), the four disulfide bridges created by the cysteine residues form a tight network which spans the entire monomer. A recent study of a native and a variant HFBI reveals the same overall structure (Hakanpää *et al.*, 2006). Furthermore, the class I hydrophobin EAS from *Neurospora crassa* has the same disulfide pairing (Kwan *et al.*, 2006). Due to the similar amino-acid sequences, monomer size and packing on an air/water interface (Kisko *et al.*, 2007), the structure of HFBIII monomer is likely to closely resemble that of HFBI and HFBII.

The interesting feature about HFBIII is the extra ninth cysteine residue. If the extra cysteine residue is used to make a disulfide bridge, it has to be an intermolecular one. Either the disulfide bridge would be such that it does not affect the aggregation of proteins (the ninth cysteine residues of neighbouring molecules are in close contact anyway) or there is no bridge. In the latter case, the extra cysteine residue would be a convenient site to chemically attach functional groups to the ordered hydrophobin monolayer.

6. Conclusions

Self-assembled films of the hydrophobin protein HFBIII were studied on an air/water interface and on a silicon substrate. The protein formed a hexagonally ordered crystalline coating on both surfaces. On the air/water interface the thickness of the film was about 30 Å and on the solid substrate the thickness of the film depends on the protein concentration. The hexagonal lattice constants $a \simeq 56$ Å were nearly equal indicating a similar arrangement of the protein molecules.

We thank Arja Kiema for technical assistance. We acknowledge the European Synchrotron Radiation Facility and HASYLAB/DESY for the provision of synchrotron radiation facilities. We thank Dr Oleg Konovalov at beamline ID10B at the ESRF and Dr Oliver H. Seeck at beamline W1 at HASYLAB for their assistance. The financial support from the Academy of Finland, National Graduate School in Material Physics, Jenny and Antti Wihuri Foundation and Emil Aaltonen Foundation (KK) and National Graduate School in Informational and Structural Biology (GRS) is gratefully acknowledged.

References

Als-Nielsen, J., Jacquemain, D., Kjaer, K., Leveiller, F., Lahav, M. & Leiserowitz, L. (1994). *Phys. Rep. Rev. Sect. Phys. Lett.* **246**(5), 251–313.
Askolin, S., Linder, M., Scholtmeijer, K., Tenkanen, M., Penttilä, M., de Vocht, M. & Wösten, H. A. B. (2006). *Biomacromolecules*, **7**, 1295–1301.
Askolin, S., Penttilä, M., Wösten, H. A. & Nakari-Setälä, T. (2005). *FEMS Microbiol. Lett.* **253**, 281–288.
Askolin, S., Turkenburg, J. P., Tenkanen, M., Uotila, S., Wilson, K. S., Penttilä, M. & Visuri, K. (2004). *Acta Cryst.* D**60**, 1903–1905.
Chen, X., Wiehle, S., Weygand, M., Brezesinski, G., Klenz, U., Galla, H.-J., Fuchs, H., Haufe, G. & Chi, L. (2005). *J. Phys. Chem. B*, **109**, 19866–19875.
Haas, H., Brezesinski, G. & Möhwald, H. (1995). *Biophys. J.* **68**, 312–314.
Hakanpää, J., Paananen, A., Askolin, S., Nakari-Setälä, T., Parkkinen, T., Penttilä, M., Linder, M. B. & Rouvinen, J. (2004). *J. Biol. Chem.* **279**(1), 534–539.
Hakanpää, J., Parkkinen, T. A. A., Hakulinen, N., Linder, M. & Rouvinen, J. (2004). *Acta Cryst.* D**60**, 163–165.
Hakanpää, J., Szilvay, G. R., Kaljunen, H., Maksimainen, M., Linder, M. & Rouvinen, J. (2006). *Protein Sci.* **15**, 2129–2140
Kisko, K., Szilvay, G., Vuorimaa, E., Lemmetyinen, H., Linder, M., Torkkeli, M. & Serimaa, R. (2007). In preparation.

Kisko, K., Torkkeli, M., Vuorimaa, E., Lemmetyinen, H., Seeck, O. H., Linder, M. & Serimaa, R. (2005). *Surf. Sci.* **584**, 35–40.
Kmetko, J., Datta, A., Evmenenko, G. & Dutta, P. (2001). *J. Phys. Chem. B*, **105**, 10818–10825.
Kwan, A., Winefield, R., Sunde, M., Matthews, J., Haverkamp, R., Templeton, M. & Mackay, J. (2006). *Proc. Natl Acad. Sci.* **103**, 3621–3626.
Lazzari, R. (2002). *J. Appl. Cryst.* **35**, 406–421.
Lenne, P.-F., Berge, B., Renault, A., Zakri, C., Vénien-Bryan, C., Courty, S., Balavoine, F., Bergsma-Schutter, W., Brisson, A., Grübel, G., Boudet, N., Konovalov, O. & Legrand, J. F. (2000). *Biophys. J.* **79**, 496–500.
Leporatti, S., Brezesinski, G. & Möhwald, H. (2000). *Colloids Surf. A Physicochem. Eng. Asp.* **161**, 159–171.
Linder, M., Selber, K., Nakari-Setälä, T., Qiao, M., Kula, M.-R. & Penttilä, M. (2001). *Biomacromolecules*, **2**, 511–517.
Linder, M. B., Szilvay, G. R., Nakari-Setälä, T. & Penttilä, M. E. (2005). *FEMS Microbiol. Rev.* **29**, 877–896.
Müller-Buschbaum, P., Hermsdorf, N., Roth, S., Wiedersich, J., Cunis, S. & Gehrke, R. (2004). *Spectrochim. Acta B*, **59**, 1789–1797.
Nakari-Setälä, T., Aro, N., Ilmén, M., Munõz, G., Kalkkinen, N. & Penttilä, M. (1997). *Eur. J. Biochem.* **248**, 415–423.
Nakari-Setälä, T., Aro, N., Kalkkinen, N., Alatalo, E. & Penttilä, M. (1996). *Eur. J. Biochem.* **235**, 248–255.
Paananen, A., Vuorimaa, E., Torkkeli, M., Penttilä, M., Kauranen, M., Lemmetyinen, H., Serimaa, R. & Linder, M. B. (2003). *Biochemistry*, **42**, 5253–5258.
Parrat, L. G. (1954). *Phys. Rev.* **95**(2), 359–369.
Renaud, G., Lazzari, R., Revenant, C., Barbier, A., Noblet, M., Ulrich, O., Leroy, F., Jupille, J., Borensztein, Y., Henry, C. R., Deville, J.-P., Scheurer, F., Mane-Mane, J. & Fruchart, O. (2003). *Science*, **300**, 1416–1419.
Ritva, S., Torkkeli, M., Paananen, A., Linder, M., Kisko, K., Knaapila, M., Ikkala, O., Vuorimaa, E., Lemmetyinen, H. & Seeck, O. (2003). *J. Appl. Cryst.* **36**, 499–502.
Seeck, O. H., Kaendler, I. D., Tolan, M., Shin, K., Rafailovich, M. H. & Sokolov, J. (2000). *Appl. Phys. Lett.* **76**(19), 2713–2715.
Szilvay, G. R., Nakari-Setälä, T. & Linder, M. B. (2006). *Biochemistry*, **45**, 8590–8598.
Torkkeli, M., Serimaa, R., Ikkala, O. & Linder, M. (2002). *Biophys. J.* **83**, 2240–2247.
Verclas, S. A., Howes, P. B., Kjaer, K., Wurlitzer, A., Weygand, M., Büldt, G., Dencher, N. A. & Lösche, M. (1999). *J. Mol. Biol.* **287**, 837–843.
Wessels, J. G. H. (1994). *Annu. Rev. Phytopathol.* **32**, 413–437.
Wetter, M.-A. van, Wösten, H. A. B., Sietsma, H. J. & Wessels, J. G. H. (2000). *Fungal Genet. Biol.* **31**, 99–104.
Wösten, H. A. B., Schuren, F. H. J. & Wessels, J. G. H. (1994). *EMBO J.* **13**(24), 5848–5854.
Wösten, H. A. B., de Vries, O. M. & Wessels, J. G. H. (1993). *Plant Cell*, **5**, 1567–1574.
Wösten, H. A. B., van Wetter, M.-A., Lugones, L. G., van der Mei, H. C., Busscher, H. J. & Wessels, J. G. H. (1999). *Curr. Biol.* **9**, 85–88.
Zhang, S. (2003). *Nature Biotechnol.* **21**(10), 1171–1178.